*Proc. Natl. Acad. Sci. USA*
Vol. 96, pp. 8461–8466, July 1999
Biophysics

# Characterization of lipid bilayer phases by confocal microscopy and fluorescence correlation spectroscopy

JONAS KORLACH*†, PETRA SCHWILLE†, WATT W. WEBB†, AND GERALD W. FEIGENSON*‡

*Section of Biochemistry, Molecular and Cell Biology and †School of Applied and Engineering Physics, Cornell University, Ithaca, NY 14853

*Contributed by Watt W. Webb, May 25, 1999*

**ABSTRACT** **We report the application of confocal imaging and fluorescence correlation spectroscopy (FCS) to characterize chemically well-defined lipid bilayer models for biomembranes. Giant unilamellar vesicles of dilauroyl phosphatidylcholine/dipalmitoyl phosphatidylcholine (DLPC/DPPC)/cholesterol were imaged by confocal fluorescence microscopy with two fluorescent probes, 1,1′-dieicosanyl-3,3,3′,3′-tetramethylindocarbocyanine perchlorate (DiI-$C_{20}$) and 2-(4,4-difluoro-5,7-dimethyl-4-bora-3a,4a-diaza-*s*-indacene-3-pentanoyl)-1-hexadecanoyl-*sn*-glycero-3-phosphocholine (Bodipy-PC). Phase separation was visualized by differential probe partition into the coexisting phases. Three-dimensional image reconstructions of confocal *z*-scans through giant unilamellar vesicles reveal the anisotropic morphology of coexisting phase domains on the surface of these vesicles with full two-dimensional resolution. This method demonstrates by direct visualization the exact superposition of like phase domains in apposing monolayers, thus answering a long-standing open question. Cholesterol was found to induce a marked change in the phase boundary shapes of the coexisting phase domains. To further characterize the phases, the translational diffusion coefficient, $D_T$, of the DiI-$C_{20}$ was measured by FCS. $D_T$ values at ~25°C ranged from $\sim 3 \times 10^{-8}$ cm$^2$/s in the fluid phase, to $\sim 2 \times 10^{-9}$ cm$^2$/s in high-cholesterol-content phases, to $\sim 2 \times 10^{-10}$ cm$^2$/s in the spatially ordered phases that coexist with fluid phases. In favorable cases, FCS could distinguish two different values of $D_T$ in a region of two-phase coexistence on a single vesicle.**

Many events that occur in cell membranes may be related to the membrane phase behavior. These events include protein sorting, protein aggregation, signaling, and membrane fusion (1, 2). For animal plasma membranes in particular, the presence of sphingolipids raises the possibility of ordered phase coexisting with fluid phase at physiological temperatures (3). Determining phase behavior is not straightforward, however, in part because of the large number of components, the small dimensions of the phases, and the possible complexity of the actual transitions (4).

In models for real biomembranes, there has been progress in mapping the phase behavior of cholesterol-containing bilayer mixtures having as many as two phospholipid components (5, 6). Because of ambiguities in the interpretation of data, we seek a direct visualization of the phase behavior. Giant unilamellar vesicles (GUVs) have proven to be useful models of biomembranes, suitable for optical microscopy (7–9). GUVs thus serve as an excellent model system for biological membranes, because they are, compared with supported bilayers, less prone to artifacts (10, 11), and they resemble cell membranes more closely than do monolayers (12, 13).

The publication costs of this article were defrayed in part by page charge payment. This article must therefore be hereby marked "*advertisement*" in accordance with 18 U.S.C. §1734 solely to indicate this fact.

PNAS is available online at www.pnas.org.

Although two-phase coexistence domains have been observed and characterized in detail in monolayers (12, 14), previous studies using bilayer systems have not resulted in a clear picture of topology where two phases coexist. Supported bilayers were shown to be prone to artifactual results (10), and previously described heterogeneities in free bilayer membranes from images of confocal sections of laurdan fluorescence (15) or wide-field fluorescence microscopy (16) exhibit relatively low resolution and do not reveal the detailed two-dimensional topology of two-phase coexistence.

Furthermore, it has been a long-standing, open question whether a phase domain in one monolayer of the lipid bilayer is exactly superimposed with a corresponding domain of the same phase in the apposing monolayer. Data obtained from fluorescence photobleaching recovery (17) were used to conclude that for some phospholipid systems the question seems to be answered positively. In contrast, lack of transbilayer coupling in phase transitions (18) or only partial coupling (19) was found by using nuclear magnetic resonance shift reagents. For supported bilayers (10), interlayer coupling has been proposed, but metastable states and constraints caused by the supporting surface have been recognized. A direct and clear demonstration of the phenomenon of interlayer coupling has not yet been described for free lipid bilayers.

In this report we describe two significant steps toward mapping the phase behavior of phospholipid/cholesterol bilayers. (*i*) By using confocal fluorescence microscopy, we have produced images that conclusively demonstrate the existence of coexisting phases. Subsequent three-dimensional image projections reveal the detailed topology of coexisting phase domains over the surface of a vesicle. The method directly enables the establishment of phase domains that are exactly superimposed in apposing monolayers. (*ii*) By using fluorescence correlation spectroscopy (FCS), we have further characterized phases by probe translational diffusion. We have been able to distinguish fluid, spatially ordered, and high-cholesterol-content phases[§] by the different values of their translational diffusion coefficient, $D_T$. Moreover, in cases in which the coexisting phases are not very dissimilar in extent,

Abbreviations: Bodipy-PC, 2-(4,4-difluoro-5,7-dimethyl-4-bora-3a,4a-diaza-*s*-indacene-3-pentanoyl)-1-hexadecanoyl-*sn*-glycero-3-phosphocholine; DiI-$C_{20}$, 1,1′-dieicosanyl-3,3,3′,3′-tetramethylindocarbocyanine perchlorate; DLPC, dilauroyl phosphatidylcholine (1,2-dilauroyl-*sn*-glycero-3-phosphocholine); DPPC, dipalmitoyl phosphatidylcholine (1,2-dipalmitoyl-*sn*-glycero-3-phosphocholine); FCS, fluorescence correlation spectroscopy; GUV, giant unilamellar vesicle; POPS, 1-palmitoyl 2-oleoyl phosphatidylserine [1-palmitoyl-2-oleoyl-*sn*-glycero-3-(phospho-L-serine)] (sodium salt).

‡To whom reprint requests should be addressed at: Section of Biochemistry, Molecular, and Cell Biology, 201 Biotechnology Building, Cornell University, Ithaca, NY 14853. e-mail: gwf3@cornell.edu.

§The term "spatially ordered phases" (often called "solid" or "gel") denotes two-dimensional spatial order in lipid bilayers that corresponds to the long-range order of three-dimensional smectic liquid crystal hydrated phases of smectic B type, and the two-dimensional fluid phases (often called "liquid-crystalline" and "liquid-ordered") that correspond to hydrated smectic A type, in which short-range order may also occur (20, 21).

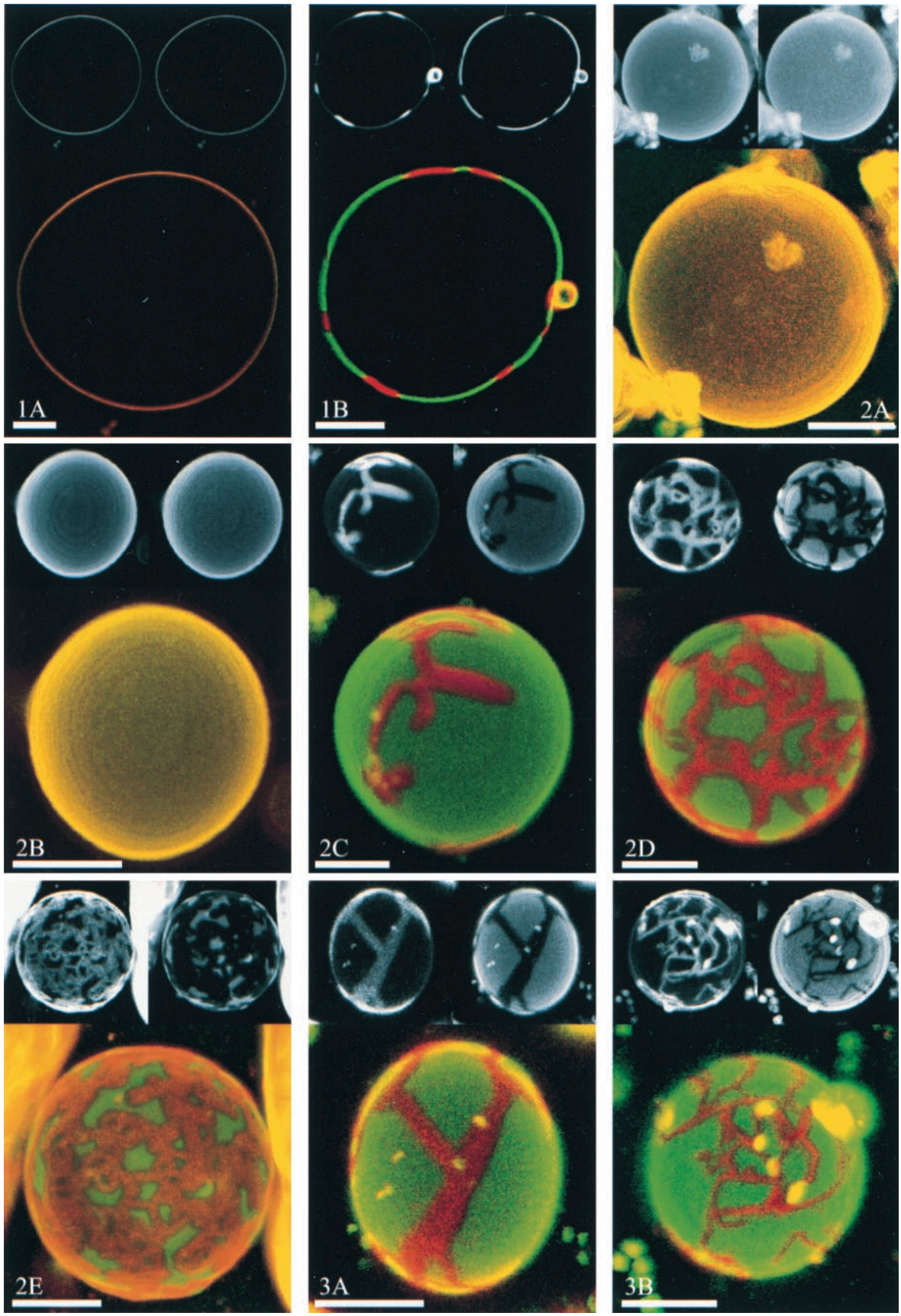


FIG. 1. The principle of lipid phase identification, showing confocal images at the equator of GUVs at a phospholipid/cholesterol composition yielding (*1A*) a single fluid phase (DLPC/DPPC = 1/0), and (*1B*) ordered-fluid two-phase coexistence (DLPC/DPPC = 0.60/0.40). In each figure, DiI-$C_{20}$ fluorescence is shown in the upper left small image and Bodipy-PC fluorescence in the upper right. Thus, the merged large lower image shows spatially ordered phase regions in red (DiI-$C_{20}$ fluorescence) and fluid phase in green (Bodipy-PC fluorescence). The asphericity of these GUVs indicates lack of osmotic stress. A small adherent vesicle is visible in *1B* and in several subsequent images. (Bars = 10 $\mu$m.)

separate values of $D_T$ can be measured for each phase on a single vesicle.

## MATERIALS AND METHODS

Phospholipids were purchased from Avanti Polar Lipids (Alabaster, AL) and cholesterol was purchased from Nu Chek Prep (Elysian, MN). The fluorescent probes 1,1′-dieicosanyl-3,3,3′,3′-tetramethylindocarbocyanine perchlorate (DiI-$C_{20}$) and 2-(4,4-difluoro-5,7-dimethyl-4-bora-3a,4a-diaza-*s*-indacene-3-pentanoyl)-1-hexadecanoyl-*sn*-glycero-3-phosphocholine (Bodipy-PC) were obtained from Molecular Probes (Eugene, OR). Purity of ≥99.5% was confirmed by thin-layer chromatography on washed, activated silica gel plates (Alltech, Deerfield, IL), developed with chloroform/methanol/water (65:25:4) for phospholipids and with petroleum ether/diethyl ether/chloroform (7:3:3) for cholesterol analysis. Phospholipid stock solutions were quantitated by phosphate assay (22).

GUVs were prepared essentially according to Akashi *et al.* (8). In all samples, 5 mol % 1-palmitoyl 2-oleoyl phosphatidylserine (POPS) was included as a charged phospholipid, necessary to obtain GUVs by this method. For confocal microscopy visualization, fluorescent probes were added to the lipid mixture at a concentration of $10^{-1}$ mol %, or $10^{-4}$ mol % for FCS. The aqueous buffer was 50 mM KCl and 5 mM Pipes, pH 7.0. Image acquisition and FCS measurements were carried out at room temperature, ~25°C. The GUVs formed were placed on deep-well slides, enclosed by a no. 1 coverslip, inverted, and allowed to settle for 10 min onto the bottom of the coverslip, where they remained stationary over the course of the experiment.

Confocal images were obtained with a MRC1024 confocal microscope (Bio-Rad) at 488 nm excitation, with emission filters of 522/35BP for Bodipy-PC and 585LP for DiI-$C_{20}$. For three-dimensional image projection of a vesicle, *z*-scans in 1-$\mu$m increments were taken through the upper half of a GUV and projected by using the software CONFOCAL ASSISTANT 4.02.

FCS measurements were carried out with a modified inverted microscope as described (23). Briefly, a 543-nm HeNe laser beam was used to epi-illuminate a 63× (1.2 numerical aperture water immersion) objective. The back aperture was underfilled to create a circular focus of ≈1 $\mu$m diameter at $e^{-2}$ relative intensity, providing 10–20 $\mu$W at the membrane. Fluorescence was collected through the objective and a collimating lens of 160-mm focal length. In the image plane, a 100-$\mu$m fiber pinhole (large enough to collect virtually all fluorescence excited by the laser illumination in its focal plane) defined the confocal volume element. The fluorescence signal was detected by an avalanche photodiode (SPCM-AQ141, EG & G, Vaudreuil, Québec, Canada), and it was correlated online with an ALV-5000 correlator card (ALV, Langen, Germany) in a host PC.

After the laser focal spot had been positioned near the center of the upper membrane of a GUV, 10 FCS measurements of 10-s duration were recorded on that location, and averaged for determination of the translational diffusion coefficient, $D_T$. FCS autocorrelation curves from each measurement interval were very reproducible, except in cases of two-phase coexistence, where sometimes only one phase component, sometimes both phases were visible during the individual 10-s interval, reflecting slight movements of the phase regions on the surface of the vesicle relative to the focal area.

The autocorrelation function $G_i(\tau)$ defined by Magde *et al.* (24) for each species *i* of independently diffusing molecules becomes for optically indistinguishable fluorophores in two dimensions:

$$G_{\text{tot}}(\tau) = \left( \sum_i \langle C_i \rangle \left( \frac{1}{1 + \tau/\tau_{d,i}} \right) \right) \Big/ A_{\text{eff}} \left( \sum_i \langle C_i \rangle \right)^2,$$

where $\langle C_i \rangle$ is the two-dimensional, time average concentration of the probe in the focal area $A_{\text{eff}}$ of ≈0.8 $\mu m^2$, $\tau_{d,i}$ the average residence time of species *i* (proportional to the inverse of the diffusion coefficient) (25). The apparatus was calibrated by measuring the known three-dimensional diffusion coefficient $D_T$ of rhodamine in solution, and the validity of the $D_T$ values obtained for the two-dimensional case of membrane diffusion was confirmed by comparison with rhodamine diffusion measured in a pseudo-two-dimensional nanostructure 250 nm in height (kindly provided by M. Foquet). Data fitting was performed with a least-squares fit algorithm (ORIGIN, Microcal, Northampton, MA). In the figures, autocorrelation amplitudes are normalized to 1 to compare the curves for their shapes and diffusion times for the different compositions. Correlation amplitudes were typically ~0.1, corresponding to an average number of fluorescent molecules in the focal area of $\langle N \rangle \sim 10$.

## RESULTS

**Confocal Imaging.** GUVs were prepared from mixtures of dilauroyl phosphatidylcholine/dipalmitoyl phosphatidylcholine (DLPC/DPPC)/cholesterol. Unilamellarity was assured by measuring the fluorescence intensity of the equator region, as described (8). Two fluorescent lipid analogs distinguished the fluid and ordered membrane phases. The partition of DiI-$C_{20}$ favors the ordered membrane phases of DPPC over coexisting fluid phases by ~3× (26). In contrast, Bodipy-PC is expected to favor the fluid phase over the DPPC ordered phases by ~4×, based on the measured partition of phospholipid analogs having a bulky moiety on an acyl chain (27). In the studies reported here, however, the precise value of the probe partition coefficient was not used, but instead the contrast in fluorescence was used simply to image the phase domains. At a given lipid composition, the GUVs that were formed had a rather uniform appearance, so that the images shown are representive of the entire sample.

Fig. 1 illustrates this principle of phase identification with a confocal microscopic section at the equator of a GUV. In this figure and in the other images shown, a single GUV was imaged by fluorescence from DiI-$C_{20}$ in the upper left, fluorescence from Bodipy-PC in the upper right, and their composite in the larger color image below. Fig. 1, *1A* shows a GUV entirely in the fluid phase (DLPC/DPPC = 1/0), having uniform fluorescence from both DiI-$C_{20}$ and Bodipy-PC. Fig. 1, *1B* shows a GUV having coexisting fluid and spatially ordered phases (DLPC/DPPC = 0.60/0.40; see below). The DiI-$C_{20}$ fluorescence in the upper left is nonuniform over the equator. For the same vesicle, the Bodipy-PC fluorescence is also nonuniform with *bright* and *dark regions exactly comple-*

(*2A–2E*) Visualization of phase separation in the binary lipid mixture of DLPC/DPPC. The images show a progression of increasing DPPC concentration relative to DLPC at DLPC/DPPC values: 1/0 (*2A*), 0.80/0.20 (*2B*), 0.60/0.40 (*2C*), 0.40/0.60 (*2D*), and 0.20/0.80 (*2E*). Note that the vesicle shown in *2D* is not unilamellar, but instead consists of two bilayers which are very close to each other. Image *2D* shows two concentric GUVs, chosen to demonstrate the principle of superposition of phase domains in apposing monolayers (see text). No GUVs were formed in pure DPPC; apparently some fluid phase must be present for successful preparations of GUVs by this method. The circular rings of contrast in these and subsequent images are due to nonuniform axial stepping between confocal images and do not indicate compositional inhomogeneities. (Bars = 10 $\mu$m.) (*3A* and *3B*) Influence of cholesterol on the two-phase region. GUVs at a constant ratio of DLPC/DPPC = 0.50/0.50 were prepared with increasing cholesterol concentrations of 0 (*3A*) and 5 mol % (*3B*). For cholesterol ≥10 mol %, images were identical in appearance to *2A* and *2B*. For explanation, see text. (Bars = 10 $\mu$m.)

Table 1. Summary of translational diffusion coefficients $D_T$ obtained from FCS measurements

| Composition, mol fraction | | | $D_T$, |
|---|---|---|---|
| DLPC | DPPC | Cholesterol | $cm^2/s$ |
| 1 | 0 | 0 | $3 \times 10^{-8}$ |
| 0.80 | 0.20 | 0 | $4 \times 10^{-8}$ |
| 0.60 | 0.40 | 0 | $5 \times 10^{-8}/2 \times 10^{-10}$ |
| 0.20 | 0.80 | 0 | $5 \times 10^{-8}/2 \times 10^{-10}$ |
| 1 | 0 | 0 | $3 \times 10^{-8}$ |
| 0.85 | 0 | 0.15 | $2 \times 10^{-8}$ |
| 0.70 | 0 | 0.30 | $1 \times 10^{-8}$ |
| 0.55 | 0 | 0.45 | $6 \times 10^{-9}$ |
| 0.40 | 0 | 0.60 | $3 \times 10^{-9}$ |
| 0.50 | 0.50 | 0 | $5 \times 10^{-8}/2 \times 10^{-10}$ |
| 0.475 | 0.475 | 0.05 | $7 \times 10^{-9}$ |
| 0.45 | 0.45 | 0.10 | $3 \times 10^{-9}$ |
| 0.425 | 0.425 | 0.15 | $3 \times 10^{-9}$ |
| 0.40 | 0 | 0.60 | $3 \times 10^{-9}$ |
| 0 | 0.40 | 0.60 | $1.5 \times 10^{-9}$ |

The relative error in determination of $D_T$ was ~20% for all compositions. In cases of two-phase coexistence, values of $D_T$ characteristic of each phase are given (if they were obtained reliably and quantitatively). Row spaces indicate separate experimental series corresponding to the component being varied (see text).

*mentary* to those of the DiI-$C_{20}$. The finding that phase identification was confirmed by two different fluorescent probes makes phase assignments more reliable.

Multibilayers in excess water of the binary mixture DLPC/DPPC at 25°C exhibit a two-phase region of coexisting ordered and fluid phases between DLPC/DPPC ~ 0.7/0.3 to ~ 0.15/0.85 (28). We obtained results consistent with this phase behavior. Fluorescence images from GUVs at increasing concentrations of DPPC are shown in Fig. 1, *2*. At DLPC/DPPC = 1/0 and 0.80/0.20 (Fig. 1, *2A* and *2B*), both DiI-$C_{20}$ and Bodipy-PC are uniformly distributed over the vesicle surface. However, at DLPC/DPPC = 0.40/0.60 (Fig. 1, *2C*), an ordered phase is visible as elongated, connected bands on the surface of the vesicles. The separate fluorescence measurements on this GUV (Fig. 1, *2C*) reveal both an enrichment of DiI-$C_{20}$ (*Upper Left*) and a depletion of Bodipy-PC (*Upper Right*) in these bands, compared with the adjacent surface region.

Continuing this series of increasing DPPC concentrations, ordered phase regions become more and more interconnected, forming a network on the vesicle surface (Fig. 1, *2D*), eventually enclosing small islands of fluid phase at DLPC/DPPC = 0.20/0.80 (Fig. 1, *2E*). In principle, we might expect to return to uniform fluorescence at higher concentrations of DPPC, but we were unable to prepare GUVs at DLPC/DPPC = 0/1 by the method used in this study.

Interestingly, in all GUV preparations studied in this series, the phase domains comprise both apposing leaflets of the bilayer in both ordered and fluid phases, thus indicating strong interlayer coupling. This finding is judged from the absence of intermediate values of fluorescence intensities for both dyes measured anywhere on the surface. For all unilamellar vesicles, only one fluorescence intensity could be measured for the fluid and ordered phase regions. If interlayer coupling did not occur, intermediate fluorescence values would be observed, because then regions would exist that were composed of one monolayer in the fluid phase and the apposing monolayer in the ordered phase (10). To highlight this point, Fig. 1, *2D* was chosen as a vesicle composed of two concentric unilamellar vesicles with their bilayers very close to each other, as established from the individual confocal image sections. In the central regions of this vesicle (where the viewing direction is nearly perpendicular, providing a clear image), areas of one (and only one) intermediate fluorescence intensity can be clearly distinguished (where one ordered bilayer and one fluid bilayer are superimposed). This intermediate fluorescence intensity is the result of the independent network of fluid and ordered phase domains in each of the adjacent bilayers.

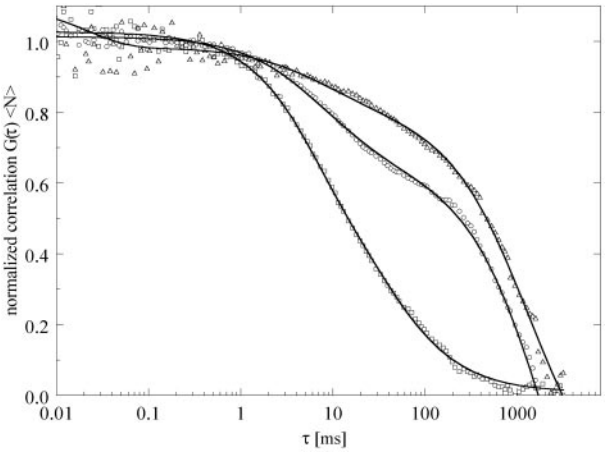


FIG. 2. Diffusion properties in laterally ordered and fluid phases in the absence of cholesterol, corresponding to Fig. 2. FCS autocorrelation curves were obtained for samples of composition DLPC/DPPC (□ = 1/0, ○ = 0.60/0.40, and △ = 0.20/0.80). Solid curves are data-fitting curves for diffusion theory from which $D_T$ values were determined. In this and all subsequent figures, correlation amplitudes are normalized to 1 by multiplying $G(\tau)$ with the average number of fluorescent molecules in the focal area $\langle N \rangle$ to compare the shapes of the curves for different compositions.

The influence of cholesterol on the two-phase region was examined by increasing the cholesterol concentration $\chi_{chol}$ from 0 to 30 mol % while keeping the ratio DLPC/DPPC = 0.50/0.50 constant (Fig. 1). When Fig. 1, *3A* and *3B* are compared, $\chi_{chol}$ = 5 mol % is seen to enhance the elongation and branching of the ordered band-like regions that were observed in the binary phospholipid mixture at high DPPC. Furthermore, the total area fraction of the ordered phase appears to be reduced for this composition. Here again, exact superposition of like phase domains is observed. At $\chi_{chol} \geq 10$ mol %, fluorescence of both dyes was uniform over the GUV surface (images not shown; their appearance was similar to that of the vesicles shown in Fig. 1, *2A* and *2B*), indicating either a single phase or heterogeneity at dimensions much smaller than the optical resolution of ~0.3 $\mu$m.

**FCS.** FCS has been applied successfully to the study of diffusion, chemistry, and photophysics of molecules in solution (24, 29, 30). In a few cases, FCS has been used to study diffusion in membranes (23, 31, 32). Two properties can be directly deduced from the autocorrelation curve of an FCS experiment: (*i*) the equilibrium average number of diffusing molecules in the laser focus volume element and (*ii*) their diffusion coefficient. Here, we make use of only the diffusion coefficient. The presence of more than one diffusing species in a sample is manifested by multiphasic curve shapes if the diffusion coefficients are sufficiently different and the amplitudes are sufficiently similar (33).

By using FCS, we measured $D_T$ on GUVs in several regions of composition; the results are summarized in Table 1. The relative error in the determination of $D_T$ was ~20% for all compositions. Representative fitting curves of the data that were used to determine $D_T$ are shown in Fig. 2 only, to retain clarity in the other figures.

The autocorrelation curves shown in Fig. 2 are for the samples corresponding to the images in Fig. 1, *2*. $D_T$ of DiI-$C_{20}$ was found to be characteristic primarily of the nature of the phase and secondarily of the lipid composition of that phase.

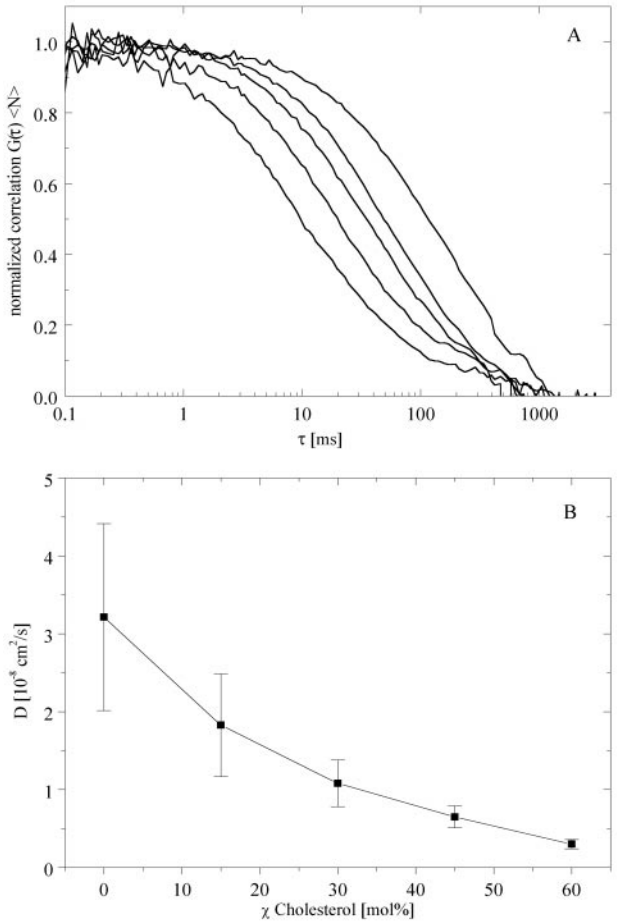


FIG. 3. The binary lipid mixture DLPC/cholesterol exhibits a continuous change in diffusion coefficient. (*A*) Autocorrelation curves at increasing cholesterol concentration are shown (from left to right) for the compositions of DLPC with 0, 15, 30, 45, and 60 mol % cholesterol. Each autocorrelation curve represents the average of five separate vesicles measured. (*B*) Average diffusion coefficients determined from the autocorrelation curves in *A*. The error bars correspond to the entire range of diffusion coefficients obtained from the individual FCS measurements.

At $\chi_{chol} = 0$ and DLPC/DPPC = 1/0, DiI-$C_{20}$ has a single $D_T \approx 3 \times 10^{-8}$ cm$^2$/s, increasing slightly to $\approx 4 \times 10^{-8}$ cm$^2$/s at DLPC/DPPC = 0.80/0.20. These values are very similar to the $D_T$ found near room temperature in other one-phase fluid bilayers (31, 34–38). In the region of two-phase coexistence (corresponding to Fig. 1, *2C*), the correlation curve shown in Fig. 2 reveals two distinct components, as obtained from averaging 10 repetitive 10-s FCS measurements on a single location of the bilayer, as described in *Materials and Methods*. We attribute the two components of DiI-$C_{20}$ diffusion for the samples of DLPC/DPPC = 0.60/0.40 to the coexisting fluid phase at composition DLPC/DPPC $\approx$ 0.7/0.3, where $D_T \approx 5 \times 10^{-8}$ cm$^2$/s and the expected spatially ordered phase at DLPC/DPPC $\approx$ 0.15/0.85, where $D_T \approx 2 \times 10^{-10}$ cm$^2$/s. Although we were unable to obtain GUVs in the pure DPPC ordered phase, we could prepare GUVs at DLPC/DPPC = 0.20/0.80, which is near the solidus boundary. Here again, $D_T \approx 2 \times 10^{-10}$ cm$^2$/s. This value of $D_T$ in an ordered lipid bilayer near room temperature is similar to that found in comparable systems (34, 35, 39). In accord with the image for this sample clearly showing some fluid phase (Fig. 1, *2E*), a fraction of fast-diffusing component (14%, $D_T \approx 5 \times 10^{-8}$ cm$^2$/s) was required to fit the autocorrelation curve. Although there is an uncertainty in the precise amount of fluid phase, FCS is sufficiently sensitive for the detection of even small amounts

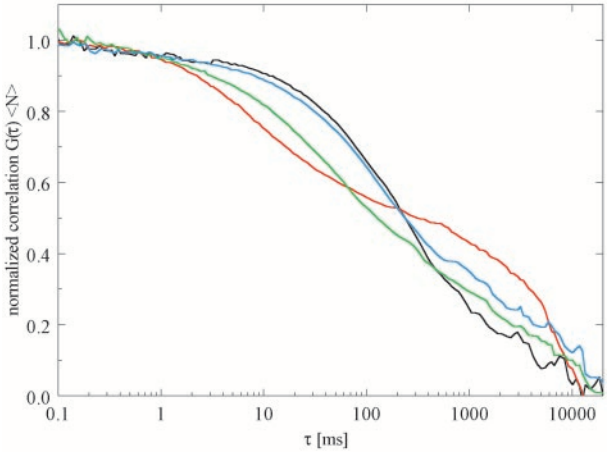


FIG. 4. FCS autocorrelation curves corresponding to the cholesterol compositions shown in Fig. 3, at constant DLPC/DPPC = 0.50/0.50. Cholesterol concentrations: red indicates 0, green indicates 5, blue indicates 10, and black indicates 15 mol %. For explanation, see text.

(~15%) of a coexisting phase that is sampled by the illuminated area.

GUVs were also examined in another binary region of composition, where DLPC/cholesterol was varied, keeping $\chi_{DPPC} = 0$. These GUVs showed no phase separation by confocal microscopy (images not shown; their appearance was similar to that of the vesicles shown in Fig. 1, *2A* and *2B*). FCS measurements revealed monophasic autocorrelation curve shapes (Fig. 3*A*), together with a gradual decrease in diffusion coefficients from $3 \times 10^{-8}$ cm$^2$/s at $\chi_{chol} = 0$, to $3 \times 10^{-9}$ cm$^2$/s at $\chi_{chol} = 60$ mol % (Fig. 3*B*). Thus, there is a decrease of the $D_T$ values with increasing cholesterol concentration, as was determined previously from measurements on phospholipid/cholesterol mixtures above the melting transition temperature of the phosphatidylcholine (31, 34).

Another interesting composition regime is that of variable $\chi_{chol}$, keeping the ratio of DLPC/DPPC constant at 0.50/0.50, which corresponds to the fluorescence images of the GUVs shown in Fig. 1, *3*. The FCS measurements on these samples (Fig. 4) show both fast ($D_T \approx 5 \times 10^{-8}$ cm$^2$/s) and slow ($D_T \approx 2 \times 10^{-10}$ cm$^2$/s) diffusion components at $\chi_{chol} = 0$. At 5 mol % cholesterol (green curve), the fast component slows to $D_T \approx 7 \times 10^{-9}$ cm$^2$/s, reflecting the increased cholesterol and DPPC content of the fluid phase. For samples containing 10 mol % cholesterol (blue curve), the fast component slows even further, to $D_T \approx 3 \times 10^{-9}$ cm$^2$/s, corresponding to a further increase in cholesterol and DPPC content in the fluid phase. Above 10 mol % cholesterol, in the composition regime in which no phase separations were resolved by confocal microscopy, the FCS correlation curves were fitted well with a single value of $D_T \approx 3 \times 10^{-9}$ cm$^2$/s. In GUVs with $\chi_{chol} \geq 5$ mol %, no slower diffusion component could be fitted quantitatively from the autocorrelation curves because the fraction of low mobility phase is small. From visual inspection of the correlation curve, however, it is clear that FCS detects small deviations from conventional single phase behavior (23).

Finally, we can compare diffusion coefficients at the very high cholesterol content of $\chi_{chol} = 60$ mol % as a function of DLPC/DPPC (see Table 1). At the extremes, in DLPC/DPPC = 1/0, $D_T \approx 3 \times 10^{-9}$ cm$^2$/s; in DLPC/DPPC = 0/1, $D_T \approx 1.5 \times 10^{-9}$ cm$^2$/s. This small range is consistent with a single phase of somewhat varying properties for probe diffusion over the entire range of DLPC/DPPC.

## DISCUSSION

Confocal fluorescence microscopy has enabled the direct observation and analysis of phase domains in GUVs. Phases

can be identified as ordered or fluid, based on the known partition behavior of appropriate fluorescent probes. Three-dimensional image projections of the confocal images reveal the morphology of coexisting ordered and fluid phase domains in GUVs with full two-dimensional resolution, thus enabling more systematic analysis of structural details as a function of composition and temperature. Furthermore, it is possible with this method to demonstrate directly whether ordered phase domains are exactly superimposed in apposing monolayers. For the two-phase regions of the lipid mixtures studied here, this was observed to be the case.

For the binary phospholipid mixture of DLPC/DPPC, a striking anisotropy of the spatially ordered phase was found in the form of very long, straight bands, with long phase boundaries sometimes extending to more than one-half the circumference of a GUV. Without attempting a detailed molecular explanation, it is clear that this topology implies an anisotropy in the molecular arrangement of the spatially ordered phase and thus in its boundary, as was previously found, e.g., in liquid crystals for the anisotropic $P_{\beta'}$ phase of dimyristoyl phosphatidylcholine (21). Anisotropy is furthermore manifested by the branching of these bands that is observed to occur with well-defined angles, usually not smaller than approximately 60°. The addition of cholesterol to this binary mixture induces an increased number of branch points, and a concomitant decrease of the widths of the bands. The increase of the fluid fractional area with cholesterol on these GUVs implies that cholesterol mediates solubilization of DPPC into the fluid phase until the entire surface is occupied by a fluid phase of high cholesterol content. As was determined by FCS analysis, this is accompanied by a decrease in the diffusion coefficient in the fluid phase.

FCS thus serves as a tool to further characterize molecular mobility in the phases systematically, with $D_T$ depending primarily on the type of phase, and secondarily on the exact phospholipid and cholesterol composition of that phase, as demonstrated in Fig. 3. In contrast to fluorescence photobleaching recovery, FCS requires only a minute concentration of fluorescent probe ($\sim 10^{-6}$ mole fraction), therefore minimally disturbing the lipid mixture under investigation. With its large dynamic range, FCS is shown to be sensitive to deviations of single-phase behavior and can yield diffusion coefficients for both phases if they coexist on a single specimen. Since there is a clear correlation to the visual images, the assignment of measured parameters becomes more reliable, strengthening this method and enabling it to look at more complex systems, such as biological membranes.

This research was carried out largely in the Developmental Resource for Biophysics Imaging Opto-Electronics with funding provided by the National Science Foundation (NSF-B1R 8800278) and the National Institutes of Health (NIH-P412 RR04224). G.W.F. is supported by the National Science Foundation (MCB-9722818). P.S. was the recipient of a fellowship of the Alexander von Humboldt Foundation.

1. Simons, K. & Ikonen, E. (1997) *Nature (London)* **387,** 569–572.
2. Edidin, M. (1997) *Curr. Opin. Struct. Biol.* **7,** 528–532.
3. Brown, D. A. & London, E. (1997) *Biochem. Biophys. Res. Commun.* **240,** 1–7.
4. Huang, J. & Feigenson, G. W. (1999) *Biophys. J.* **76,** 2142–2157.
5. Silvius, J. R., del Giudice, D. & Lafleur, M. (1996) *Biochemistry* **35,** 15198–15208.
6. Almeida, P. F. F., Vaz, W. L. C. & Thompson, T. E. (1993) *Biophys. J.* **64,** 399–412.
7. Schneider, M. B., Jenkins, J. T. & Webb, W. W. (1984) *Biophys. J.* **45,** 891–899.
8. Akashi, K., Miyata, H., Itoh, H. & Kinosita, K. (1996) *Biophys. J.* **71,** 3242–3250.
9. Moscho, A., Orwar, O., Chiu, D. T., Modi, B. P. & Zare, R. N. (1996) *Proc. Natl. Acad. Sci. USA* **93,** 11443–11447.
10. Seul, M., Subramaniam, S. & McConnell, H. M. (1985) *J. Phys. Chem.* **89,** 3592–3595.
11. Sackmann, E. (1996) *Science* **271,** 43–48.
12. McConnell, H. M. (1991) *Annu. Rev. Phys. Chem.* **42,** 171–195.
13. Keller, S. L. & McConnell, H. M. (1998) *Phys. Rev. Lett.* **81,** 5019–5022.
14. McConnell, H. M., Tamm, L. K. & Weis, R. M. (1984) *Proc. Natl. Acad. Sci. USA* **81,** 3249–3253.
15. Parasassi, T., Gratton, E., Yu, W. M., Wilson, P. & Levi, M. (1997) *Biophys. J.* **72,** 2413–2429.
16. Haverstick, D. M. & Glaser, M. (1987) *Proc. Natl. Acad. Sci. USA* **84,** 4475–4479.
17. Almeida, P. F. F., Vaz, W. L. C. & Thompson, T. E. (1992) *Biochemistry* **31,** 7198–7210.
18. Sillerud, L. O. & Barnett, R. E. (1982) *Biochemistry* **21,** 1756–1760.
19. Schmidt, C. F., Barenholz, Y., Huang, C. & Thompson, T. E. (1978) *Nature (London)* **271,** 775–777.
20. DeGennes, P. G. & Prost, J. (1993) in *The Physics of Liquid Crystals* (Oxford Univ. Press, London), pp. 18–40.
21. Schneider, M. B., Chan, W. K. & Webb, W. W. (1983) *Biophys. J.* **43,** 157–165.
22. Kingsley, P. B. & Feigenson, G. W. (1979) *Chem. Phys. Lipids* **24,** 135–147.
23. Schwille, P., Korlach, J. & Webb, W. W. (1999) *Cytometry* **36,** 176–182.
24. Magde, D., Elson, E. & Webb, W. W. (1972) *Phys. Rev. Lett.* **29,** 705–708.
25. Schwille, P., Meyer-Almes, F. J. & Rigler, R. (1997) *Biophys. J.* **72,** 1878–1886.
26. Spink, C. H., Yeager, M. D. & Feigenson, G. W. (1990) *Biochim. Biophys. Acta* **1023,** 25–33.
27. Huang, N., Florine-Casteel, K., Feigenson, G. W. & Spink, C. (1988) *Biochim. Biophys. Acta* **939,** 124–130.
28. Van Dijck, P. W. M., Kaper, A. J., Oonk, H. A. J. & De Gier, J. (1977) *Biochim. Biophys. Acta* **470,** 58–69.
29. Eigen, M. & Rigler, R. (1994) *Proc. Natl. Acad. Sci. USA* **91,** 5740–5747.
30. Maiti, S., Haupts, U. & Webb, W. W. (1997) *Proc. Natl. Acad. Sci. USA* **94,** 11753–11757.
31. Fahey, P. F., Koppel, D. E., Barak, L. S., Wolf, D. E., Elson, E. L. & Webb, W. W. (1977) *Science* **195,** 305–306.
32. Rigler, R. (1995) *J. Biotechnol.* **41,** 177–186.
33. Meseth, U., Wohland, T., Rigler, R. & Vogel, H. (1999) *Biophys. J.* **76,** 1619–1631.
34. Rubinstein, J. L. R., Smith, B. A. & McConnell, H. M. (1979) *Proc. Natl. Acad. Sci. USA* **76,** 15–18.
35. Alecio, M. R., Golan, D. E., Veatch, W. R. & Rando, R. R. (1982) *Proc. Natl. Acad. Sci. USA* **79,** 5171–5174.
36. Vaz, W. L. C., Clegg, R. M. & Hamilton, D. (1985) *Biochemistry* **24,** 781–786.
37. Shin, Y.-K. & Freed, J. H. (1989) *Biophys. J.* **55,** 537–550.
38. Almeida, P. F. F., Vaz, W. L. C. & Thompson , T. E. (1992) *Biochemistry* **31,** 6739–6747.
39. Fahey, P. F. & Webb, W. W. (1978) *Biochemistry* **17,** 3046–3053.